Research Article Vol. 34, No. 3 / 9 Feb 2026 / Optics Express 5472
Optics EXPRESS

Long-range OFDR distributed strain sensing based on optimized deskew filter and image denoising methods

CAILING FU,[1,2] NIANQING ZOU,[1,2] HUAJIAN ZHONG,[1,2] RONGYI SHAN,[1,2] YABO SHI,[1,2] HUAFENG ZHA,[1,2] LIJIE WANG,[1,2] YONGZHENG XU,[1,2] WEIJIA BAO,[1,2] YIPING WANG,[1,2] AND CHANGRUI LIAO[1,2,*]

[1]*Shenzhen Key Laboratory of Photonic Devices and Sensing Systems for Internet of Things, Guangdong and Hong Kong Joint Research Centre for Optical Fiber Sensors, State Key Laboratory of Radio Frequency Heterogeneous Integration, Shenzhen University, Shenzhen 518060, China*
[2]*Shenzhen Key Laboratory of Ultrafast Laser Micro/Nano Manufacturing, Key Laboratory of Optoelectronic Devices and Systems of Ministry of Education/Guangdong Province, College of Physics and Optoelectronic Engineering, Shenzhen University, Shenzhen 518060, China*
[*]*cliao@szu.edu.cn*

Abstract: A method combining an optimized deskew filter based on a peak-seeking algorithm and an image denoising based on Gaussian filtering was proposed, enabling a strain sensing with a spatial resolution of 5 cm over a measurement range of 1.68 km. In the optimized deskew filter method, the accurate estimation of the nonlinear phase was improved by third-order Taylor expansion and high-accuracy estimation of the time delay in the auxiliary interferometer using a peak-searching method. By employing an optimized deskew filter based on the peak-searching method, the amplitude and width of the peak located at 1212.16 m were improved from 5.9 dB and 45 cm to 14.4 dB and 7 cm, respectively. The strain distribution at 1212 m could be clearly identified at a spatial resolution of 5 cm with the Gaussian filtering-based image denoising method, when the strain was increased from 500 to 2000 με.

1. Introduction

Optical frequency domain reflectometry (OFDR) has been widely used in various fields, such as small-range structural health monitoring [1] and 3D shape sensing [2], due to its high spatial resolution, large measurement range, and no measurement dead zone. However, in some scenarios, such as monitoring the shape of submarine cables [3] and wind turbine blade [4], it is necessary to maintain a kilometer-level test length and thousands of με-levels at centimeter-level spatial resolution. The key to ensuring high-performance OFDR distributed sensing was the linear tuning of the tunable laser source (TLS) during frequency sweeping. Nevertheless, the frequency sweep of the TLS suffered from the unavoidable nonlinearity, which seriously limited the measurement distance of OFDR system [5]. Thus, much efforts have been focused on how to compensate for phase noise and achieve long-range OFDR. In 2013, a simple method, i.e., deskew filter, was proposed to compensate for the tuning nonlinearity of TLS, achieving a measurable range of 10 km at a spatial resolution of 20 cm [6]. Subsequently, an optimized deskew filter method based on cepstrum was proposed to achieve a spatial resolution of 80 cm within a measurable range of 80 km [7]. The combination of moving average filter and third-order Taylor expansion was employed to provide high-precision estimation of periodic phase noise, where the spatial resolution was 535 μm over the measurement range of 8 km [8]. In addition to the effort in extending the distance and improving the spatial resolution, long-range OFDR has gained great attention in distributed sensing. For example, independent component analysis source-noise

#586367 https://doi.org/10.1364/OE.586367
Journal © 2026 Received 2 Dec 2025; revised 17 Jan 2026; accepted 17 Jan 2026; published 5 Feb 2026

Optics EXPRESS

separation method was proposed to handle the random noise, achieving an effective strain sensing distance of 75 m with a spatial resolution up to 2 mm [9]. And shape-adaptive principal component analysis Block-Matching three-dimensional filter image denoising was presented to effectively suppress noise aggravation along with an increasing of the sensing distance, where a distributed strain sensing with a 5 cm spatial resolution was achieved on a 200 m all grating fiber [10]. Furthermore, a spectral splicing method was proposed for OFDR distributed strain sensing, which achieved a strain sensitivity of ±3.2 με over a length of 1 km with a spatial resolution of 1 cm and extended the strain measurement range to 10,000 με [11]. Phase-noise-compensated OFDR was applied to extend the measurement distance to 1.5 km with a spatial resolution of 10 cm [12].

In this paper, a method combining an optimized deskew filter based on peak-seeking algorithm and an image denoising based on Gaussian filtering was proposed, enabling a strain sensing with a spatial resolution of 5 cm over a measurement range of 1.68 km. In the optimized deskew filter method, the accurate estimation of the nonlinear phase was improved by third-order Taylor expansion and high-accuracy estimation of the time delay in the auxiliary interferometer using peak-searching method.

The principles of the optimized deskew filter with peak-seeking algorithm for nonlinear phase estimation and image denoising method with Gaussian filtering for OFDR strain demodulation were firstly elaborated. Subsequently, the effect of Taylor expansion order on the nonlinear phase estimation accuracy of the main interferometer was investigated. Moreover, the nonlinear phase and distance domain signals were compared using deskew filter method based on nominal delay fiber length and optimized deskew filter method based on peak-seeking. Finally, further comparisons were conducted between image denoising methods with and without Gaussian filtering to evaluate their performance in long-range strain demodulation.

2. Principle of optimized deskew filter based on peak-seeking algorithm

2.1. Theory of OFDR

The linear frequency sweeping light generated by the tunable laser source (TLS) was split into two paths: one path was entered the fiber under test (FUT) for measurement, while the other was used as a local reference path, as shown in Fig. 1. The light reflected by the FUT due to Rayleigh scattering or Fresnel reflection was interfered with the reference light to generate a beat frequency signal. Here, the optical field of the local reference light, i.e., $E_r(t)$, could be given by

$$E_r(t) = E_0 \exp\{j[2\pi f_0 t + \pi\gamma t^2 + 2\pi e(t)]\} \tag{1}$$

where *E0* is the amplitude of the light field, f_0 and γ is the initial light frequency and tuning speed of the TLS, $e(t)$ is the nonlinear phase or phase noise of the TLS. Assuming that there is a reflection point at the position of z of the FUT, the optical field of the received signal, i.e., $E_s(t)$, could be given by

$$\begin{aligned} E_s(t) &= \sqrt{R(\tau)}E_r(t-\tau) \\ &= \sqrt{R(\tau)}E_0 \exp\{j[2\pi f_0(t-\tau) + \pi\gamma(t-\tau)^2 + 2\pi e(t-\tau)]\}, \end{aligned} \tag{2}$$

where $R(\tau)$ is the attenuation coefficient, τ is the time delay between the reference light and the reflection point at the z-position of the FUT, $\tau = 2nz/c$. Here, the $E_r(t)$ and $E_s(t)$ could be considered as the local oscillator (LO) signal, i.e., reference signal, and received signal from FUT, i.e., measurement signal, respectively. Thus, the beat frequency signals generated by the

Optics EXPRESS

interference of the LO and received signals, after removing the direct term, could be expressed as

$$I(t) = 2\sqrt{R(\tau)}E_0^2 \cos\left\{2\pi\left[f_0\tau + f_b t + \frac{1}{2}\gamma\tau^2 + e(t) - e(t-\tau)\right]\right\}, \tag{3}$$

where $f_b = \gamma\tau$ is the beat frequency rate, and $e(t) - e(t-\tau)$ is a nonlinear phase noise term of the TLS.

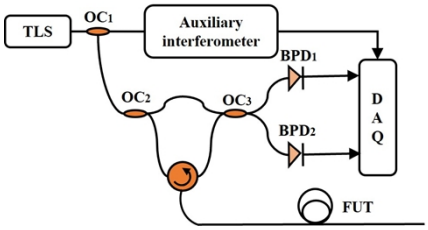

Fig. 1. Experimental setup of simple OFDR. TLS: tunable laser source; OC: optical coupler; BPD: balanced photodetector; FUT: fiber under test; DAQ: data acquisition.

2.2. Principle of optimized deskew filter

Assuming the nonlinear phase term of the LO in the main interferometer, i.e., $e(t)$, was known, a Hilbert transformation was performed on Eq. (3) to convert it into the complex exponential form, which could be given by

$$I(t) = 2\sqrt{R(\tau)}E_0^2 exp\left[j2\pi\left(f_0\tau + f_b t + \tfrac{1}{2}\gamma\tau^2\right)\right] S_e(t)S_e^*(t-\tau), \tag{4}$$

where $S_e(t) = exp[j2\pi e(t)]$ and $S_e(t-\tau) = exp[j2\pi e(t-\tau)]$, and the symbol * represents complex conjugate. Based on Eq. (4), when the nonlinear phase, i.e., $e(t)$, was accurately estimated from auxiliary interferometer, the distance independent nonlinear phase term of the LO light, i.e., $S_e(t)$, could be eliminated through multiplication, i.e.,

$$I_1(t) = I(t)S_e^*(t) = 2\sqrt{R(\tau)}E_0^2 exp\left[j2\pi\left(f_0\tau + f_b t + \frac{1}{2}\gamma\tau^2\right)\right] S_e^*(t-\tau). \tag{5}$$

However, the nonlinear phase term, i.e., $S_e(t-\tau)$, was distance dependent, which could not be removed by a single reference function. Therefore, a distance-dependent time-shift, namely a deskew filter of $\exp(j\pi f^2/\gamma)$, was applied to the beat frequency signal, i.e., $I_1(t)$, in a frequency domain,

$$I_2(t) = F^{-1}\{F\{I_1(t)\}\exp(j\pi f^2/\gamma)\}, \tag{6}$$

where F and F^{-1} denotes the Fourier transform and inverse Fourier transform, respectively. Substituting Eq. (5) into Eq. (6), the expression for $I_2(t)$ could be obtained as

$$I_2(t) = 2\sqrt{R(\tau)}E_0^2 \exp[j2\pi(f_0\tau + f_b t)]S(t), \tag{7}$$

where $S(t) = F^{-1}\{F\{S_e(t)\}\exp(j\pi f^2/\gamma)\}$. Then the term of $S_e^*(t-\tau)$ could be converted into a distance-independent term. From Eq. (5), the linear beat frequency signals at any delay time τ could be recovered after removing $S(t)$, i.e., multiplying with $S^*(t)$, which could be given as

$$I_3(t) = I_2(t)S^*(t) = 2\sqrt{R(\tau)}E_0^2 exp[j2\pi(f_0\tau + f_b t)]. \tag{8}$$

Therefore, the nonlinearity effect could be completely eliminated provided that the LO nonlinear phase of the TLS, i.e., $e(t)$, was accurately estimated using optimized deskew filter

Optics EXPRESS

algorithm, as shown in Fig. 2. The nonlinear phase term, i.e., $e(t)$, could be estimated from an auxiliary interferometer with a constant reference time delay, i.e., τ_{ref}. Then the normalized beat frequency signal, i.e., I_{AI}(t), could be expressed as

$$I_{AI}(t) = cos\left\{2\pi\left[f_0\tau_{ref} + \gamma\tau_{ref}t + \frac{1}{2}\gamma\tau_{ref}^2 + e(t) - e(t-\tau_{ref})\right]\right\}. \tag{9}$$

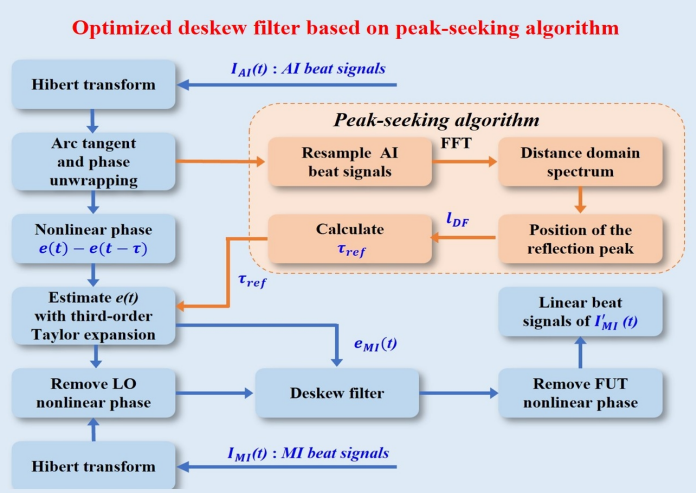

Fig. 2. Flowchart of an optimized deskew filter method based on peak-seeking algorithm for long-range OFDR. $I_{AI}(t)$: beat frequency signal of auxiliary interferometer; $I_{MI}(t)$: beat frequency signal of main interferometer; $e(t) - e(t - \tau_{ref})$: nonlinear phase term of auxiliary interferometer; l_{DF}: delay fiber length; τ_{ref}: time delay of auxiliary interferometer; $e_{MI}(t)$: estimated nonlinear term of main interferometer; $I'_{MI}(t)$: compensated beat frequency signal of main interferometer; FFT: fast Fourier transform.

By performing Hilbert transform, arc tangent, and phase unwrapping operation on the Eq. (9), the nonlinear phase term, i.e., $e(t) - e(t - \tau)$, could be obtained. Usually, the time delay of the auxiliary interferometer, i.e., τ_{ref}, was small. There is the same nonlinear noise in the main interferometer and auxiliary interferometer, originating from the same TLS. Then the nonlinear phase of the MI could be estimated by using the nonlinear phase noise of the AI. The nonlinear phase of the reference arm of the MI, i.e., $e_{MI}(t)$, could be estimated through Taylor expansion, given by

$$e(t) - e(t - \tau_{ref}) \approx e'_{MI}(t)\tau_{ref}, \tag{10}$$

where $e'_{MI}(t)$ is the derivative of $e_{MI}(t)$ with respect to time t. Thus, the estimation of nonlinear phase could be expressed as

$$e_{MI}(t) = \int \frac{e(t) - e(t - \tau_{ref})}{\tau_{ref}} dt = \int \frac{\varphi(t)}{\tau_{ref}} dt. \tag{11}$$

The compensation effect of the deskew filter algorithm was dependent on the estimation accuracy of $e_{MI}(t)$. Here, high-order Taylor expansion was carried out to improve the accuracy, which could be given by [8]

$$e_{MI}(t) = \int [\frac{\varphi(t)}{\tau_{ref}} + \frac{1}{2}\frac{d\varphi(t)}{dt} + \frac{\tau_{ref}}{12}\frac{d^2\varphi(t)}{dt^2} - \frac{{\tau_{ref}}^3}{720}\frac{d^4\varphi(t)}{dt^4}]dt. \tag{12}$$

Optics EXPRESS

2.3. Estimation of time delay in the auxiliary interferometer, i.e., τ_{ref}, based on peak-seeking algorithm

The term of time delay in the auxiliary interferometer, i.e., τ_{ref}, could be expressed as

$$\tau_{ref} = \frac{2nl}{c}, \tag{13}$$

where n is the effective refractive index of the single mode fiber (SMF) with a value of 1.46, i.e., $n = 1.46$, l is the length of delay fiber in the auxiliary interferometer, and c is the speed of light in vacuum, i.e., $c = 3 \times 10^8\ m/s$. Based on Eq. (13), the accuracy of the τ_{ref} was only dependent on the length of delay fiber. In order to accurately obtain the delay fiber length, a peak-seeking algorithm was proposed, as shown in the orange dashed box in Fig. 2. Firstly, the Hilbert transform was performed on the beat frequency signal of auxiliary interferometer to obtain the complex signal. Secondly, the arc tangent and phase unwrapping operations were conducted to obtain the phase information. Then the obtained phase information was resampled at equal phase intervals on the beat frequency signal of auxiliary interferometer, and transformed it into the distance domain through fast Fourier transform (FFT). Finally, the accurate length of delay fiber, i.e., position of the reflection peak, could be obtained by searching the peak. In this way, the τ_{ref} could be accurately estimated by peak-seeking algorithm.

3. Principle of OFDR strain demodulation based on image denoising method

To improve the performance of long-range OFDR strain sensing, an image denoising method based on the Gaussian filtering algorithm was proposed, as shown in Fig. 3. Firstly, two optical frequency-domain beat signals corresponding to different states, i.e., reference (Ref.) signal without strain and measurement (Mea.) signal with strain, were acquired and compensated using aforementioned optimized deskew filter method. Secondly, FFT was performed to convert these signals from the frequency domain to the distance domain. Thirdly, the FUT was divided into multiple sections for the Ref. and Mea. signal by using a sliding window. And each sliding window at the same position was transformed back to frequency domain through inverse FFT (IFFT), and were padded zeros to a size of 2^{15}. Subsequently, the cross-correlation between Ref. and Mea. signal was performed to obtain cross-correlation profile. One-dimensional (1D) cross-correlations along the fiber could be obtained by traversing the entire fiber, which were arranged in order of corresponding positions to construct a three-dimensional (3D) cross-correlation of peak position-distance-amplitude [13]. Then the peak position-distance plane was projected along the amplitude dimension to obtain a two-dimensional (2D) cross-correlation map that

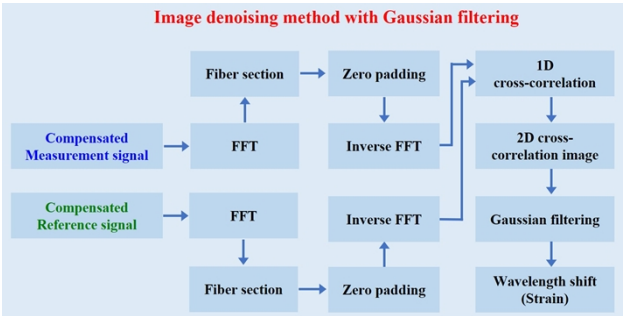

Fig. 3. OFDR strain demodulation with image denoising method based on Gaussian filtering. Compensated measurement/Reference signal: the signal compensated using an optimized deskew filter method based on peak-seeking algorithm.

Optics EXPRESS

could be used for strain demodulation. Note that each pixel was a pair of the cross-correlation value and its spatial position, and the color was the strength of the pixel value. The abnormal points in 2D image were usually treated as noise point, which could be effectively removed and smoothed by Gaussian filtering. Therefore, the Gaussian filtering was applied to denoise the 2D image. Finally, the strain could be accurately demodulated using the wavelength shift.

4. Experimental setup and results

4.1. OFDR experimental setup

To verify the effectiveness of the proposed optimized deskew filter and image denoising method, a conventional OFDR with kilometer-level FUT length was constructed. As shown in Fig. 4, the linear frequency sweeping light generated by the TLS was split into two paths by an optical coupler (OC_1). Note that the sweeping range and sweeping rate of the TLS was 1550~1570 nm and 20 nm/s, respectively. One path was entered the auxiliary Mach-Zehnder interferometer consisting of a delay fiber, i.e., local reference path, to generate an auxiliary interference signal for phase noise estimation and compensation. Note that the nominal length of the delay fiber was 95 m, i.e., l_{DF} = 95 m. Another path was entered the MI including FUT for measurement. In the MI, another OC_4 was used to inject one arm of the circulator (CIR) connected to the FUT and the other arm where the polarization controller (PC) was located, respectively. Note that the FUT was connected by two SMFs through a flange with corresponding lengths of l_1 and l_2, and its interface type was angled physical contact (APC). A polarization diversity detection, including two polarization beam splitters (PBSs), i.e., PBS_1 and PBS_2, as well as two BPDs, i.e., BPD_1 and BPD_2, was employed to reduce the polarization fading effects in the MI. The main and auxiliary interference signals were converted to electrical signals by three balanced photodetectors (BPDs) and acquired via a data acquisition card (DAQ). Note that the sampling rate of DAQ was set to 125 MHz based on the sweeping rate and kilometer-level length FUT.

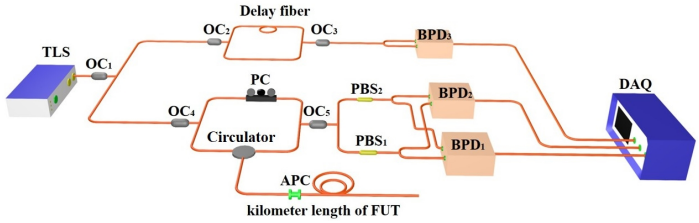

Fig. 4. Experimental setup of conventional OFDR for kilometer-level FUT lengths. PC: polarization controller: Faraday rotating mirror; PBS: polarization beam splitter; APC: angled physical contact.

4.2. Phase compensation based on optimized deskew filter method with peak-seeking

To investigate the effect of Taylor expansion order on the estimation accuracy of $e_{MI}(t)$, the Taylor expansion curve of each term in Eq. (12) was firstly studied under the FUT length of 1212 m. As shown in Fig. 5(a), the curve of the 1st term was relatively smooth, attributing to low-frequency component of $e_{MI}(t)$. Compared with the 1st term in Fig. 5(a), the smoothness of the second term was decreased due to small fluctuations, indicating that more accurate nonlinear phase could be estimated through the detail information contained in the fluctuations. The reason was that the details represented by high-frequency components began to appear under high-order Taylor expansion. The amplitudes of the 3rd and 4th terms was sharply dropped to the order of 10^{-19} and 10^{-36}, respectively, as shown in Figs. 5(c) and 5(d), resulting from higher power of τ_{ref} in the third and fourth term. At this time, the effective signal was easily affected by background noise

Optics EXPRESS

and submerged in the noise, making it impossible to accurately estimate the nonlinear phase. Theoretically, the higher the Taylor expansion order, the more accurate the estimation. However, the high-order noise was also equally introduced. Based on the noise level, i.e., the amplitude of noise and high-frequency components, the third-order Taylor expansion was ultimately selected to compensate phase.

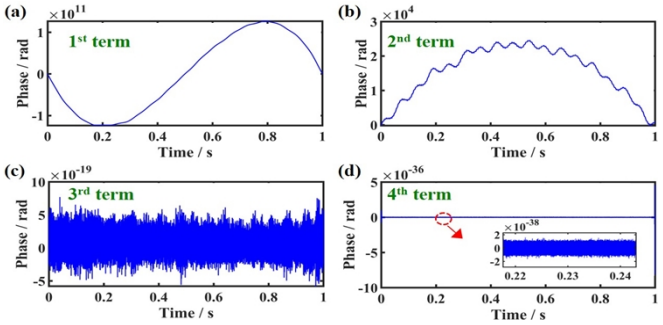

Fig. 5. Phase expansion results of each term in Eq. (12): (a) 1st term, (b) 2nd term, (c) 3rd term, and (d) 4th terms.

Then, the nonlinear phase and distance domain signals under third-order Taylor expansion were estimated and compared using deskew filter based on nominal delay fiber length and optimized deskew filter based on peak-seeking. As shown in Fig. 6(a), the maximum amplitude of the un-compensated nonlinear phase was as high as 0.92×10^5 rad, where the amplitude difference between the maximum and minimum amplitudes was 1.69×10^5 rad. Subsequently, the maximum amplitude and amplitude difference of the nonlinear phase was improved to 0.87×10^5 and 1.59×10^5 rad, using deskew filter based on the nominal length of delay fiber, i.e., $l_{DF(n)} = 95$m. This indicated that the nonlinear phase suppression was limited using the deskew filter method without peak-seeking algorithm. In contrast, the maximum amplitude and amplitude difference was further improved to 0.44×10^5 and 0.92×10^5 rad using optimized deskew filter, i.e., with peak-seeking algorithm. Compared to the non-compensation and compensation with deskew filter method, the phase information of the beat signal obtained by optimized deskew filter was reduced to 0.05×10^7 rad, corresponding to the suppressed nonlinear phase, as shown in Fig. 6(b).

As shown in Fig. 7(a), no reflection peak was observed in the distance domain spectrum without phase compensation, indicating that the Fresnel reflection from APC connections and connectors could not be detected due to the nonlinearity of the TLS frequency tuning. As shown in Figs. 7(b) and 7(c), the first Fresnel reflection at position of 208.98 m, i.e., Peak_1, could be clearly identified, where the width of the peak was 4 cm. However, the amplitude and the width of the far-end reflection peak at the position of 1212.16 m, i.e., Peak_2, was 5.90 dB and 45 cm, respectively. Obviously, the amplitude was too weak to be detected. The reason was that inaccurate estimation of the nonlinear phase of the main interferometer, i.e., $e_{MI}(t)$, using the deskew filter method based on nominal length of delay fiber.

To achieve long-range OFDR, the optimized deskew filter method based on peak-seeking algorithm was adopted to accurately calculate the delay fiber length in auxiliary interferometer. Firstly, the length of delay fiber in the auxiliary interferometer was determined to be 94.8869 m, i.e., $l_{DF(c)} = 94.8869$m, using peak-seeking algorithm, as shown in Fig. 8(a). According to Eq. (13), the time delay was calculated to be $9.2356e^{-7}$, i.e., $\tau_{ref} = 9.2356e^{-7}$s. Compared with the cepstrum method [7], only one FFT was required for peak-seeking method, reducing the computational burden. Then the nonlinear phase of main interferometer, i.e., $e_{MI}(t)$, was re-estimated and incorporated it into the deskew filter algorithm. This indicated that the nonlinear phase was effectively suppressed using optimized deskew filter based on peak-seeking algorithm.

Optics EXPRESS

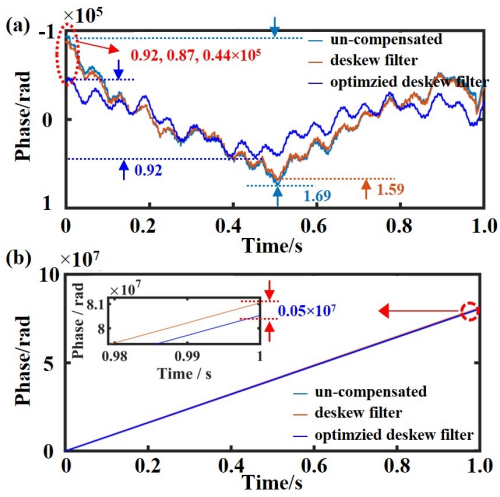

Fig. 6. Phase of the beat frequency signal estimated using third-order Taylor expansion: (a) nonlinear phase; (b) total phase. The light blue, orange, and dark blue curves corresponded to the results of uncompensated, the deskew filtering method based on nominal delay fiber length, and the optimized peak-seeking-based deskew filtering method, respectively.

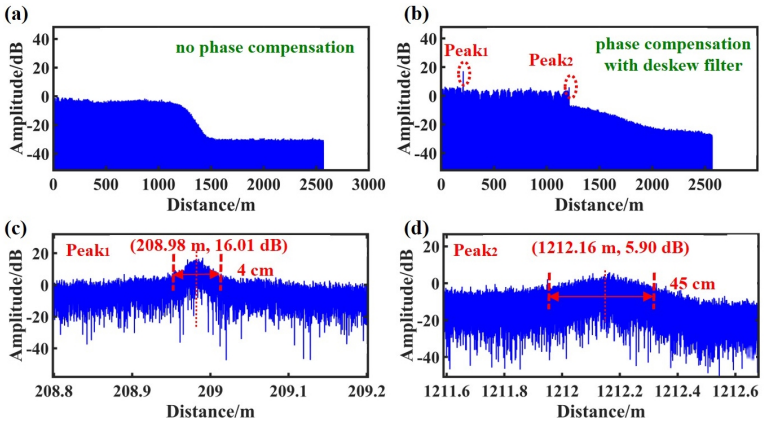

Fig. 7. (a) Uncompensated distance domain spectrum; (b) distance domain spectrum after phase compensation using the deskew filter method based on nominal delay fiber length; (c-d) enlarged views of peak$_1$ and peak$_2$ in Fig. 7(b).

Optics EXPRESS

Then, the two Fresnel reflection peaks located at 208.98 m and 1212.16 m were clearly observed, as shown in Figs. 8(b-d). Moreover, the amplitude and width of the $peak_2$ was improved to 14.4 dB and 7 cm, respectively. The amplitude and width of $Peak_1$ were comparable, regardless of using the deskew filter and optimized deskew filter. The spectral broadening of $Peak_2$ caused by nonlinear phase noise could be effectively suppressed using optimized deskew filter, i.e., improving from 45 cm to 7 cm. Note that the lengths of the two SMFs of FUT were approximately 209 and 1003 m, corresponding to a total length of 1212 m. Therefore, the optimized deskew filter method based on peak-seeking algorithm was suitable for kilometer level OFDR.

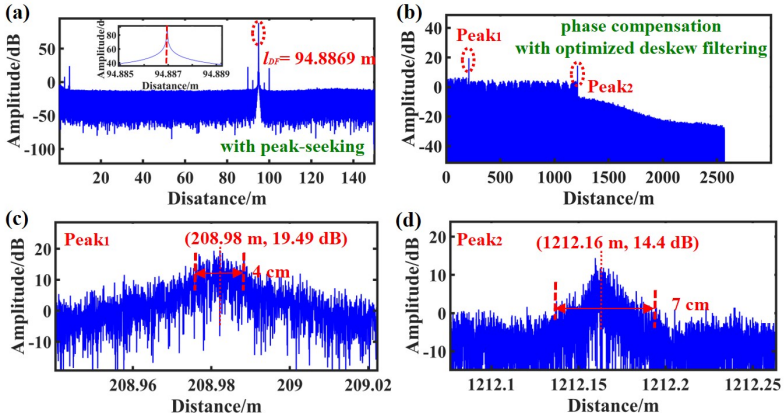

Fig. 8. (a) Distance domain spectrum of the delay fiber in the auxiliary interferometer obtained using the peak-seeking algorithm; (b) distance domain spectrum after phase compensation using an optimized deskew filter based on peak-seeking algorithm; enlarged views of (c) $peak_1$ and (d) $peak_2$ in Fig. (b).

4.3. Long-range strain demodulation based on image denoising method with Gaussian filtering

Finally, the image denoising method with or without Gaussian filtering were studied and compared to demodulate the long-range strain demodulation. Firstly, the strain was applied to the end 1 m of the FUT with a length of approximately 1212 m, corresponding to the position of 1211.73~1212.70 m. Note that one end of the SMF was fixed, other end was fixed on a 1D translation stage to apply the strain along the fiber axis. And the strain was increased from 500 to 2000 με with a step of 500 με. As shown in Fig. 9(a), a large amount of high-frequency noise and multiple false peaks were observed in the 2D cross-correlation spectrum using image denoising method without Gaussian filtering, when the applied strain was 2000 με. Similarly, a large fluctuation of the demodulated strain was observed, indicating that the signal was submerged in noise when the applied strain was 2000 με, as shown in Fig. 9(b). Compared with Fig. 9(a), the spectral surface was smooth and the peak-to-peak contrast was enhanced, as shown in Fig. 9(c). And a regular rectangular strain distribution was successfully demodulated using image denoising method with Gaussian filtering, as shown in Fig. 9(d). Note that the kernel size and standard deviation were set to 5×5 and 3, respectively. This indicated that the strain signal of 2000 με at position of 1212 m could be accurately recovered from the noise by combing optimized deskew filter methods with image denoising methods based on Gaussian filtering at the spatial resolution of 5 cm. Moreover, the strain variation in the zero-strain section, i.e., accuracy of the demodulated strain with Gaussian filtering, was ± 4 με, as shown in inset of Fig. 9(d). When the applied strain was less than 500 με, the strain distribution could be clearly demodulated without Gaussian filtering, as shown in Fig. 9(e). However, the signal was submerged in noise when the

Optics EXPRESS

applied strain was 2000 με. In addition, there was wrong points at the position of 1063.63 m in the zero-strain section. Compared with Fig. 9(e), the strain distribution in the stretched-strain section, corresponding to position of 1210.73 to 1211.70 m, could be clearly identified without wrong point in the zero-strain section, as shown in Fig. 9(f). This indicated that the strain sensing performance could be greatly improved by using image denoising based on Gaussian filtering.

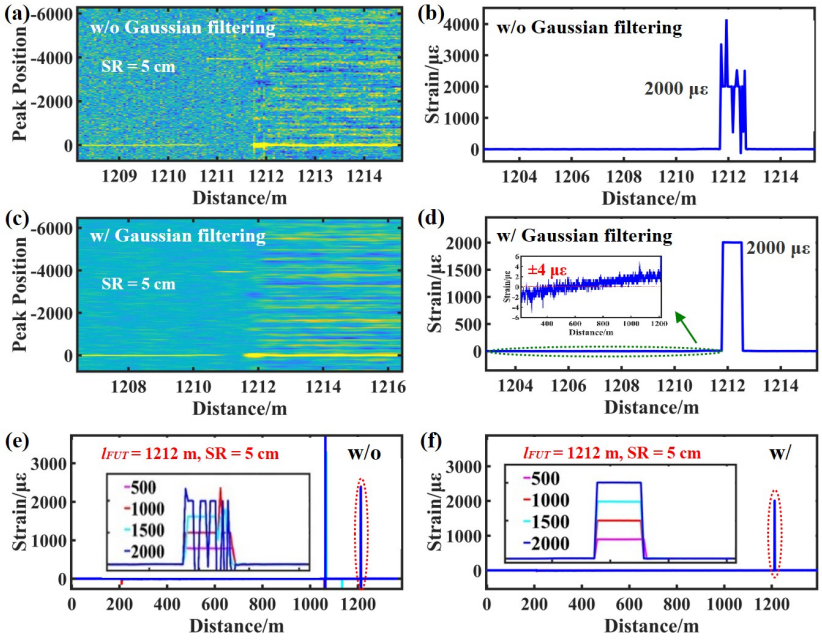

Fig. 9. Demodulated strain profiles under 2000 με strain: (a-b) without Gaussian filtering and (c-d) with Gaussian filtering; demodulated strain profiles as strain increased from 500 to 2000 με: (e) without Gaussian filtering and (f) with Gaussian filtering. Note that the strain was applied at the position of 1212 m and the spatial resolution was 5 cm.

To further evaluate the reliability of the optimized deskew filter and image denoising in kilometer-level OFDR strain sensing, the FUT with a length of approximately 1680 m was employed. Compared with the un-compensated distance domain spectrum without peaks, the amplitudes of the three peaks at positions of 1003.87, 1210.66, 1686.65 m were 37.98, 7.45, and 1.99 dB, respectively, as shown in Fig. 10(a). Similarly, the stretched-strain section was completely submerged by noise, making it impossible to identify the applied strain, as shown in Fig. 10(b). In addition, the number of wrong points was increased in the zero-strain section, resulting from the nonlinear phase noise and attenuated Rayleigh scattering that increased with distance. As shown in Fig. 10(c), the strain distribution was successfully demodulated in the zero- and stretched-strain section at the spatial resolution of 5 cm by using image denoising method, indicating that a strain of 1300 με at the position of 1685 m could be achieved by using optimized deskew filter and image denoising method.

Optics EXPRESS

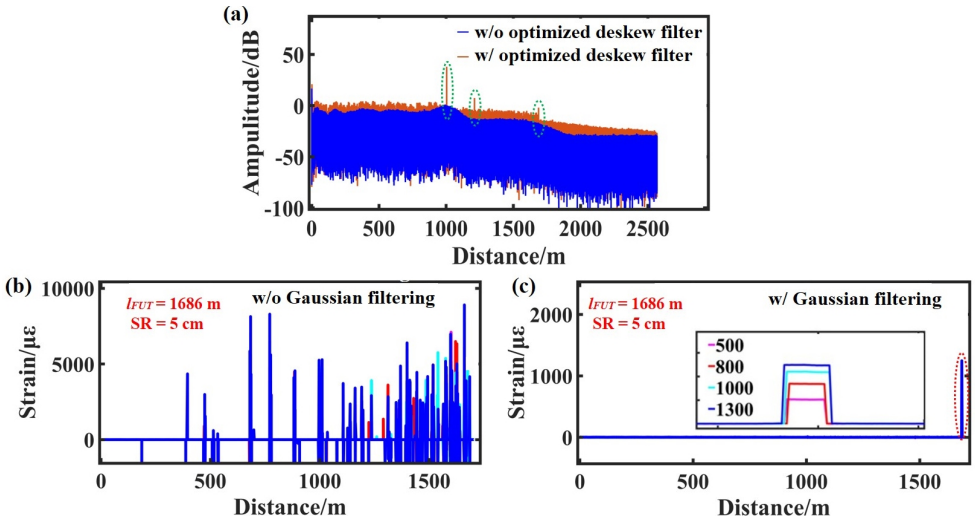

Fig. 10. (a) Uncompensated distance domain spectrum and distance domain spectrum after phase compensation using an optimized deskew filter based on peak-seeking, labeled by the blue and orange curves, respectively; demodulated strain profiles as strain increased from 500 to 1300: (b) without Gaussian filtering and (c) with Gaussian filtering. Note that the strain was applied at the position of 1686 m and the spatial resolution was 5 cm.

5. Conclusion

In conclusion, the optimized deskew filter method based on a peak-seeking algorithm was demonstrated to improve the amplitude and width of reflection peaks in long-range OFDR. The amplitude and width of the first Fresnel reflection at position of 208.98 m, i.e., $Peak_1$, were comparable, regardless of using the deskew filter method based on nominal length of delay fiber and optimized deskew filter method based on peak-seeking. Notably, the amplitude and width of the second peak located at 1212.16 m, i.e., $Peak_2$, was improved from 5.9 dB and 45 cm to 14.4 dB and 7 cm, respectively. The reason was that the nonlinear phase was accurate estimated by third-order Taylor expansion and high-accuracy estimation of the time delay in the auxiliary interferometer, i.e., $9.23e^{-7}$ s, using peak-searching method. Moreover, the strain distribution in the stretched-strain section, corresponding to position of 1211.73 to 1212.70 m, was clearly identified without wrong point in the zero-strain section using image denoising method based on Gaussian filtering under the spatial resolution of 5 cm, when the strain was increased from 500 to 2000 με. Furthermore, the strain distribution of 1300 με was also successfully demodulated, when the FUT was extended to 1685 m.

Funding. National Key Research and Development Program of China (2023YFB3209500); National Natural Science Foundation of China (grant nos. U22A2088, 62375178, 62405196); Shenzhen Science and Technology Program (JCYJ20241202124226032); LingChuang Research Project of China National Nuclear Corporation (No. CNNC-LCKY-202265); China Postdoctoral Science Foundation (grant nos. 2024M752107).

Disclosures. The authors declare no conflicts of interest.

Data availability. Data underlying the results presented in this paper are not publicly available at this time but may be obtained from the authors upon reasonable request.

References

1. X. Zhou, "Fast OFDR demodulation method for tunnel crack monitoring," Chin. J. Sens. Technol **38**(8), 1425–1431 (2025).
2. C. Fu, Z. Peng, P. Li, *et al.*, "Progress in OFDR-based distributed optical-fiber temperature/strain/shape sensing," Laser Optoelectron. Prog **60**(11), 100–110 (2023).

Optics EXPRESS

3. S. Yang, Q. Zhang, and X. Wei, "Research and application status of distributed monitoring technology for submarine optical cables," Mod. Transm **3**, 41–44 (2023).
4. D. Jian, H. Zhang, J. Li, *et al.*, "Strain measurement of the quasi-static heterotypic wind turbine blade using OFDR," Optoelectron. Lett 1–5 (2025).
5. Z. Guo, J. Yan, G. Han, *et al.*, "High sensing accuracy realization with millimetre/sub-millimetre resolution in optical frequency domain reflectometer," J. Lightwave Technol. **40**(12), 4050–4056 (2022).
6. Z. Dong, X. S. Yao, T. Liu, *et al.*, "Compensation of laser frequency tuning nonlinearity of a long-range OFDR using deskew filter," Opt. Express **21**(3), 3826–3834 (2013).
7. Y. Du, Y. Liu, Z. Ding, *et al.*, "Method for improving spatial resolution and amplitude by optimized deskew filter in long-range OFDR," IEEE Photonics J. **6**(5), 1–11 (2014).
8. C. Zou, C. Lin, T. Mou, *et al.*, "Beyond a 10^7 range-resolution-^{1} product in an OFDR based on a periodic phase noise estimation method," Opt. Lett. **47**(20), 5373–5376 (2022).
9. S. Li, Y. Xu, Z. Liu, *et al.*, "High spatial resolution OFDR system based on independent component analysis algorithm for long-range distributed strain measurement," J. Lightwave Technol. **42**(5), 1716–1724 (2024).
10. M. Pan, P. Hua, Z. Ding, *et al.*, "Long-distance distributed strain sensing in OFDR by BM3D-SAPCA image denoising," J. Lightwave Technol. **40**(24), 7952–7960 (2022).
11. T. Zhu, C. Lin, J. Yang, *et al.*, "Improve accuracy and measurement range of sensing in km-level OFDR using spectral splicing method," Opt. Express **31**(13), 20980–20993 (2023).
12. R. Ogu, D. Tanimura, C. Zhang, *et al.*, "Long-range static and dynamic strain measurement by using phase-noise-compensated OFDR," J. Lightwave Technol. **42**(18), 6240–6245 (2024).
13. S. Zhao, J. Cui, Z. Wu, *et al.*, "Accuracy improvement in OFDR-based distributed sensing system by image processing," IOptics and Lasers in Engineering **124**, 105824 (2020).